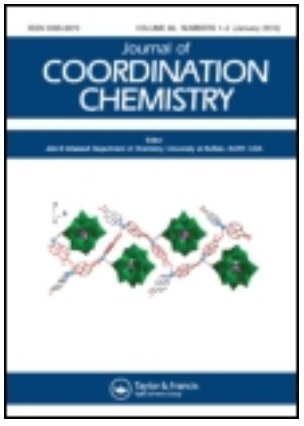

Journal of Coordination Chemistry
Publication details, including instructions for authors and subscription information:
http://www.tandfonline.com/loi/gcoo20

An ion-pair complex [TTF][Pd(mnt)$_2$]: synthesis, crystal structure, magnetic property, and electrical conductivity

Can Wang [a], Guo-Jun Yuan [a], Wei-Hua Ning [a], Jian-Lan Liu [a] & Xiao-Ming Ren [a b]

[a] State Key Laboratory of Materials-Oriented Chemical Engineering and College of Science, Nanjing University of Technology, Nanjing, PR China

[b] State Key Laboratory & Coordination Chemistry Institute, School of Chemistry and Chemical Engineering, Nanjing University, Nanjing, PR China

Accepted author version posted online: 24 May 2013.Published online: 26 Jun 2013.

To cite this article: Can Wang, Guo-Jun Yuan, Wei-Hua Ning, Jian-Lan Liu & Xiao-Ming Ren (2013) An ion-pair complex [TTF][Pd(mnt)$_2$]: synthesis, crystal structure, magnetic property, and electrical conductivity, Journal of Coordination Chemistry, 66:14, 2529-2540, DOI: 10.1080/00958972.2013.808337

To link to this article: http://dx.doi.org/10.1080/00958972.2013.808337

Journal of Coordination Chemistry, 2013
Vol. 66, No. 14, 2529–2540, http://dx.doi.org/10.1080/00958972.2013.808337

An ion-pair complex [TTF][Pd(mnt)$_2$]: synthesis, crystal structure, magnetic property, and electrical conductivity

CAN WANG†, GUO-JUN YUAN†, WEI-HUA NING†, JIAN-LAN LIU† and XIAO-MING REN*†,‡

†State Key Laboratory of Materials-Oriented Chemical Engineering and College of Science, Nanjing University of Technology, Nanjing, PR China
‡State Key Laboratory & Coordination Chemistry Institute, School of Chemistry and Chemical Engineering, Nanjing University, Nanjing, PR China

(*Received 14 December 2012; in final form 2 April 2013*)

A new ion-pair complex, [TTF][Pd(mnt)$_2$] (**1**), where TTF^+ = tetrathiafulvalene and mnt^{2-} = maleonitriledithiolate, was synthesized and characterized structurally. Compound **1** crystallizes in triclinic space group *P-1*, with $a = 8.008(5)$ Å, $b = 11.333(8)$ Å, $c = 11.373(6)$ Å, $\alpha = 108.112(7)°$, $\beta = 91.550(5)°$, $\gamma = 95.232(5)°$, and $V = 975.2(11)$ Å^3. The $[TTF]^+$ cations (C) and $[Pd(mnt)_2]^-$ anions (A) form mixed stacks in …AACCAACC… fashion, and the neighboring mixed stacks are held together via van der Waals forces in the crystal. Compound **1** shows weak Curie/Weiss-type magnetic behavior from 2 to 370 K; theoretical investigation disclosed the existence of strongly antiferromagnetic coupling in both $[Pd(mnt)_2]_2^{2-}$ and $[TTF]_2^{2+}$ dimer pairs via frontier orbitals overlap mechanism and weakly ferromagnetic coupling between the face-to-face overlapped $[TTF]^+$ and $[Pd(mnt)_2]^-$ via spin polarization mechanism within a mixed stack. The powdered pellet electrical conductivity measurement indicated that **1** shows semiconductor character with activation energy of 1.1(3) eV.

Keywords: Palladium-bis-maleonitriledithiolene; Tetrathiafulvalene; Crystal structure; Magnetic property; Electrical conductivity

1. Introduction

The planar metal-bis-maleonitriledithiolate (abbr. as $[M(mnt)_2]^-$, where M = Ni, Pd, and Pt) complexes have been widely studied with the conjugated system in $[M(mnt)_2]^-$ extending across the entire molecule, and corresponding ion-pair compounds display versatile structural and physical properties [1–9].

The ion-pair arrangement in the $[M(mnt)_2]^-$ crystal, directly related to physical properties, is strongly affected by the nature of the countercation. Salts of $[M(mnt)_2]^-$ (where M is Ni, Pd, or Pt) with small cations exhibit unusual cooperative phenomena in the solid state. For instance, $[NH_4][Ni(mnt)_2]\cdot H_2O$ exhibits properties of a Heisenberg antiferromagnetic chain at room temperature but the ground state is a singlet with the monoanions associated as dimers at low temperatures [10, 11]. This insulator salt, $[NH_4][Ni(mnt)_2]\cdot H_2O$, with localized spins shows long-range ferromagnetic order below 4.5 K and the Curie temperature demarcating the transition to ferromagnetic order abruptly

*Corresponding author. Email: xmren@njut.edu.cn

disappears at 6.8 kbar [1]. The non-stoichiometric compound, $[H_3O]_{0.33}Li_{0.8}[Pt(mnt)_2]\cdot 1.67H_2O$, exhibits metallic properties at room temperature but undergoes the Peierls instability at ~220 K to become a semiconductor [12, 13]. The non-stoichiometric compound, $Cs_{0.82}[Pd(mnt)_2]\cdot 0.5H_2O$, is the first palladium dithiolene complex to exhibit metallic behavior under pressure [2].

In our previous studies, the Λ-shaped benzylpyridinium derivatives, with flexible molecule conformation, have been combined with $[Ni(mnt)_2]^-$ to give a series of 1-D spin-Peierls-type compounds [14–19], and the isostructural spin-Peierls-type $[Pt(mnt)_2]^-$ ion-pair compounds were also obtained in some cases if $[Ni(mnt)_2]^-$ was replaced by $[Pt(mnt)_2]^-$ in the corresponding $[Ni(mnt)_2]^-$ ion-pair compound [20]; however, ion-pair compounds of $[Pd(mnt)_2]^-$ with benzylpyridinium derivatives always display different packing structure from the $[Ni(mnt)_2]^-$ analogs [21, 22]. The similar structure feature was also observed in the charge-transfer salts of TTF derivatives with $[M(mnt)_2]^-$ (M = Ni, Pd, and Pt) [9]. These observations demonstrated that the electronic feature of $[M(mnt)_2]^-$ (M = Ni, Pd, and Pt) has an effect on the ion-pair alignment in the crystal besides the structural nature of countercation.

The planar tetrathiafulvalene (TTF^+) and its derivative cations have been used to constitute a wide class of organic materials famous for their transport properties, ranging from insulating through semiconducting to metallic and superconducting feature [5–9, 23]. In addition, 1-D spin-Peierls transition molecule-based magnets comprised of TTF^+ were also reported [24, 25]. However, only 20 crystal structures of compounds that contain TTF parts and $[M(mnt)_2]^-$ have been found in the Cambridge Structural Database. Among these, only two involved TTF^+ [26].

In this paper, the planar tetrathiafulvalene cation ($[TTF]^+$) was selected to combine with $[Pd(mnt)_2]^-$ to produce a new ion-pair compound $[TTF][Pd(mnt)_2]$, with crystal structure, magnetic, and conductive properties investigated.

2. Experimental

2.1. *Chemicals and reagents*

All chemicals and reagents were purchased from commercial sources and used without purification. The starting materials, tetrathiafulvalenium tetrafluoroborate ($[TTF]_3[BF_4]_2$) [27] and the tetrabutylammonium bis(maleonitrile-dithiolato)palladate ($[Bu_4N][Pd(mnt)_2]$) [28], were synthesized following published procedures.

2.2. *Physical measurements*

C, H, and N analyses were performed with an Elementar Vario EL III analytic instrument. Powder X-ray diffractions (PXRD) were collected on a Bruker D8 diffractometer with Cu Kα radiation (λ = 1.54018 Å). The acceleration voltage was 40 kV with a 40 mA current flux. Scatter and diffraction slits of 0.5 mm and collection slits of 0.3 mm were used and data were collected from 2θ 5° to 50°, with a scanning rate of 4°/min and a sample interval of 0.02°. Magnetic susceptibility data for polycrystalline sample were measured from 2 to 370 K using a Quantum Design MPMS-5S superconducting quantum interference device magnetometer and the diamagnetic susceptibility was not removed. Electrical conductivity measurements for the compressed powder pellet were made using a Keithley 2440 5A source meter.

2.3. *Preparation of [TTF][Pd(mnt)$_2$] (1)*

The crystals of [TTF][Pd(mnt)$_2$] were obtained using diffusion within a bilayer environment; the more dense CH_3CN solution of [Bu_4N][Pd(mnt)$_2$] with a little I_2 was deposited at the bottom of a test tube and the less dense CH_3CN solution with [TTF]$_3$[BF_4]$_2$ was slowly put on top of the CH_3CN solution of [Bu_4N][Pd(mnt)$_2$] and then the tube was sealed. Black single crystals were grown on the tube wall after 30 days and the yield was ca. 70%. No pure [TTF][Pd(mnt)$_2$] was obtained, if there is not a little I_2. Elemental analyses for C, H, and N: Calcd for $C_{14}H_4N_4S_8Pd$ (%): C, 28.4; N, 9.5; H, 0.68. Found: C, 27.7; N, 9.1; H, 0.66. IR spectrum (KBr disk, cm^{-1}): 3062(s) and 3039(s) arose from $\nu_{C\text{-}H}$ of $[TTF]^+$; 2206(s) assigned to $\nu_{C\equiv N}$ of mnt^{2-} ligands.

2.4. *Density functional theory calculation details*

All density functional theory (DFT) calculations were carried out utilizing the Gaussan98 program [29] on an SGI 3800 workstation. Single-point energy calculations of the triplet and broken-symmetric states for $[Pd(mnt)_2]_2^{2-}$, $[TTF_2]^{2+}$, and $[TTF]^+[Pd(mnt)_2]^-$ spin dimers in 1 were performed on the nonmodelized molecular geometry from single-crystal X-ray analysis, and the SCF convergence criterion is 10^{-8}. In this study, the generalized gradient approximations (bpw91 [30–35]) with the lanl2dz basis sets were employed.

2.5. *X-ray crystallography*

The single-crystal X-ray diffraction data for [TTF][Pd(mnt)$_2$] were collected using a Bruker SMART APEX CCD diffractometer with graphite-monochromated Mo Kα radiation ($\lambda = 0.71073$ Å) at $T = 296(2)$ K. Data reductions and absorption corrections were performed with SAINT and SADABS software packages [36]. The structure was solved by direct methods and refined on F^2 by full-matrix least-squares with SHELXTL-97 [37]. All non-hydrogen atoms were refined anisotropically. Crystallographic data and structure refinement parameters are summarized in table 1.

3. Results and discussion

3.1. *Crystal structure description*

Ion-pair compound **1** crystallizes in the triclinic space group *P-1*, as shown in figure 1. An asymmetric unit consists of one $[Pd(mnt)_2]^-$ with one $[TTF]^+$ and the typical bond lengths and angles are listed in table 2. Generally, the Pd–S bond lengths are somewhat shorter in $[Pd(mnt)_2]^-$ than those in $[Pd(mnt)_2]^{2-}$, since the HOMO of $[Pd(mnt)_2]^-$/$[Pd(mnt)_2]^{2-}$ exhibits anti-bonding character between Pd and S atoms; the averaged Pd–S distance is about 2.277 Å in $[Pd(mnt)_2]^-$ [38–40], while ca. 2.295 Å in $[Pd(mnt)_2]^{2-}$ [41, 42]. The Pd–S bond lengths are 2.273(3)–2.289(3) Å and S–Pd–S bite angles, 90.23(9)° and 90.19(9)°, are close to 90° in $[Pd(mnt)_2]^-$. These bond parameters are comparable to values in reported $[Pd(mnt)_2]^-$ compounds [21, 22]. The bond lengths and angles fall within the expected range in the planar $[TTF]^+$ (table 2).

As displayed in figure 2, $[Pd(mnt)_2]^-$ (A) and $[TTF]^+$ (C) form the mixed stack in …AACCAACC… fashion along the crystallographic *a–b* direction. The neighboring

Table 1. Crystal data and structure refinement for **1**.

Chemical formula	$C_{14}H_4N_4S_8Pd$
CCDC	884,505
Formula weight	591.09
Temperature (K)	296(2)
Wavelength (Å)	0.71073
Crystal system	Triclinic
Space group	*P-1*
a (Å)	8.008(5)
b (Å)	11.333(8)
c (Å)	11.373(6)
α (°)	108.112(7)
β (°)	91.550(5)
γ (°)	95.232(5)
V (Å^3)/Z	975.2(11)/2
Density (g cm^{-3})	2.013
Absorption coefficient (mm^{-1})	1.817
F(000)	580
Data collection θ range	1.89–25.00
Index range	$-9 \leqslant h \leqslant 9$ $-13 \leqslant k \leqslant 12$ $-13 \leqslant l \leqslant 13$
Reflections collected	6993
Independent reflections	3396
R_{int}	0.040
Absorption correction	Semi-empirical from equivalents
Refinement method on F^2	Full-matrix least-squares
Data/restraints/parameters	3396/0/244
Goodness-of-fit on F^2	1.014
Final R indices [I > 2σ(I)]	$R1 = 0.0709$, w$R2 = 0.1905$
R indices (all data)	$R1 = 0.0996$, w$R2 = 0.$ 0.2074
Residual/(e Å^{-3})	3.156/−0.895

$R_1 = \Sigma(||F_0| - |F_c||)/\Sigma|F_0|$; $wR_2 = \Sigma w(|F_0|^2 - |F_c|^2)^2/\Sigma w\ (|F_0|^2)^2]^{1/2}$.

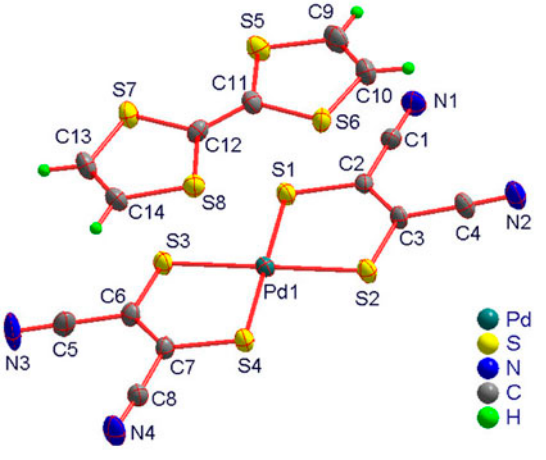

Figure 1. Molecular structure of **1** with non-hydrogen atom labeling and displacement ellipsoids at the 30% probability level.

Table 2. Bond lengths and angles in **1**.

$[Pd(mnt)_2]^-$ anion		$[TTF]^+$ cation	
Bond length/Å			
Pd1–S1	2.277(3)	S5–C9	1.696(12)
Pd1–S2	2.284(3)	S5–C11	1.717(11)
Pd1–S3	2.289(3)	S6–C10	1.719(11)
Pd1–S4	2.273(3)	S6–C11	1.735(10)
S1–C2	1.711(9)	S7–C13	1.703(10)
S2–C3	1.709(9)	S7–C12	1.729(9)
S3–C6	1.707(10)	S8–C12	1.707(9)
S4–C7	1.729(9)	S8–C14	1.714(11)
N1–C1	1.149(13)	C9–C10	1.349(16)
N2–C4	1.125(12)	C11–C12	1.386(14)
N3–C5	1.132(13)	C13–C14	1.348(15)
N4–C8	1.116(13)		
C1–C2	1.410(14)		
C2–C3	1.401(13)		
C3–C4	1.447(12)		
C5–C6	1.455(13)		
C6–C7	1.374(13)		
C7–C8	1.456(14)		
Bond angle/°			
∠S4–Pd1–S2	89.86(9)	∠C9–S5–C11	96.2(5)
∠S1–Pd1–S2	90.23(9)	∠C10–S6–C11	95.5(5)
∠S4–Pd1–S3	90.19(9)	∠C13–S7–C12	95.3(5)
∠S1–Pd1–S3	89.72(9)	∠C12–S8–C14	95.5(5)
∠S4–Pd1–S1	179.48(9)	∠C10–C9–S5	117.4(9)
∠S2–Pd1–S3	179.70(9)	∠C9–C10–S6	116.6(9)
∠N1–C1–C2	178.7(12)	∠C12–C11–S5	124.5(8)
∠N2–C4–C3	176.3(11)	∠C12–C11–S6	121.2(8)
∠N3–C5–C6	177.6(11)	∠S5–C11–S6	114.3(5)
∠N4–C8–C7	176.6(11)	∠C11–C12–S8	123.2(7)
		∠C11–C12–S7	121.6(8)
		∠S8–C12–S7	115.1(6)
		∠C14–C13–S7	117.2(8)
		∠C13–C14-S8	116.8(8)

anion and cation are almost parallel to each other within a mixed stack, where the mean molecular planes, defined by S1, S2, S3, and S4 for $[Pd(mnt)_2]^-$ *versus* S5, S6, S7, and S8 for $[TTF]^+$, make 1.38° dihedral angle, and the long molecular axes of $[Pd(mnt)_2]^-$ anion and $[TTF]^+$ cation make 3.87° angle. Adjacent mixed stacks are spread in the directions of both the long and the short molecular axes of anion and cation to give 3-D supramolecular network via shorter S…S and N…S contacts (figure 3).

As illustrated in figure 4(a), shorter interatomic contacts are observed within an eclipsed anion dimer and an eclipsed cation dimer as well with $d_{Pd1\ldots Pd1\#1} = 3.458$, $d_{S1\ldots S4\#1} = 3.439$, $d_{S2\ldots S3\#1} = 3.447$, $d_{S5\ldots S8\#2} = 3.439$, $d_{S6\ldots S7\#2} = 3.423$, and $d_{C12\ldots C11\#2} = 3.400$ Å, where the hash-marked atoms are symmetrically generated and the corresponding symmetric codes: #1 = 1 − *x*, −*y*, 1−*z*; #2 = −*x*, 1−*y*, 1−*z*. These distances are less than the van der Waals radii summations for two adjacent atoms. In reported $[Pd(mnt)_2]^-$ compounds, formation of eclipsed $[Pd(mnt)_2]_2^{2-}$ dimer pair is favored and the intermolecular Pd…Pd distances range from 3.329 to 3.456 Å with nearest neighboring intermolecular S…S distances of 3.336–3.42 Å in the intra-dimer [21, 22, 42]. Thus, the intermolecular Pd…Pd and S…S distances within $[Pd(mnt)_2]_2^{2-}$ in **1** are comparable to the corresponding values reported.

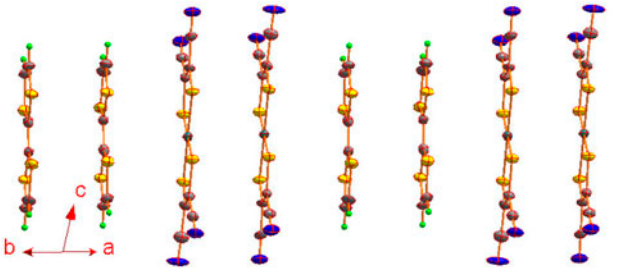

Figure 2. Mixed stack in a fashion of …AACCAACC… along the crystallographic *a–b* direction in the crystal of **1**.

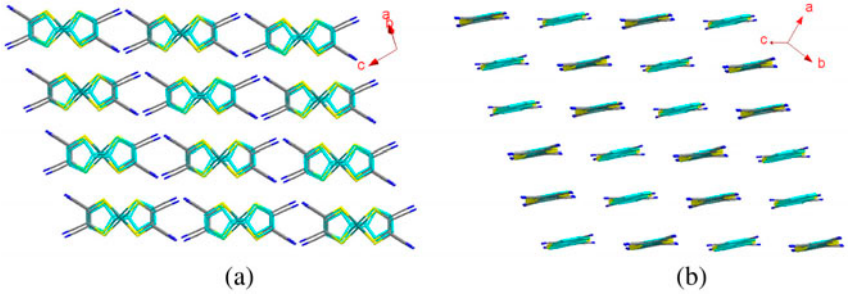

Figure 3. Packing diagrams viewed along the different directions for **1**.

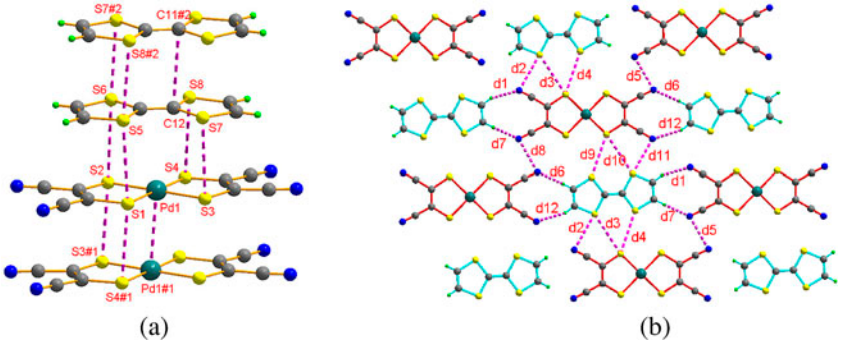

Figure 4. Illustration for typical interatomic distances in **1** (a) within a mixed stack and referred to the main text (b) between the neighboring anions and cations in both directions of the long and short molecular axes of anion and cation with d1 = 2.486, d2 = 3.389, d3 = 3.800, d4 = 3.706, d5 = 3.178, d6 = 2.363, d7 = 2.325, d8 = 3.178, d9 = 3.689, d10 = 3.782, d11 = 3.297 and d12 = 2.493 Å, respectively.

Typical interatomic distances between the neighboring anion and cation, with $d_{S1\ldots S5} = 3.768$, $d_{S2\ldots S6} = 3.887$, $d_{S3\ldots S7} = 3.779$, and $d_{S4\ldots S8} = 3.904$ Å within a mixed stack, are longer than those within a dimer of anion/cation. Figure 4(b) shows the shorter interatomic contacts between the neighboring anions and cations in both directions of the long and short molecular axes of anion and cation, and these distances are slightly longer than the van der Waals radii summations for two adjacent atoms besides d2, d5, d8, and d11.

3.2. *Magnetism*

Variations of magnetic susceptibility (χ_m) with temperature are displayed in figure 5 for **1**, where χ_m is the magnetic susceptibility per [TTF][Pd(mnt)$_2$] unit. This ion-pair compound shows Curie/Weiss-type magnetic behavior, thus, equation (1) was used for fits of magnetic susceptibility,

$$\chi_m = \frac{C}{T-\theta} + \chi_0 \quad (1)$$

The χ_0 term includes the core diamagnetism and the possible van Vleck paramagnetism; the symbols C and θ represent Curie and Weiss constants, respectively. The best fit for the magnetic susceptibility data in the range 2–370 K gave the corresponding parameters, $C = 1.66(6) \times 10^{-2}$ emu K M^{-1}, $\theta = -1.4(2)$ K, and $\chi_0 = 6.7(2) \times 10^{-4}$ emu M^{-1}, respectively. Small Curie constant, being approximately equal to the 4.4% $S = ½$ spin-only value, and Weiss constant indicated (1) the weak Curie/Weiss-type paramagnetism originates from magnetic impurity, which is related to defects of unpaired $[TTF]_2^{2+}$ and $[Pd(mnt)_2]_2^{2-}$ units and (2) there exists a $S = 0$ ground state with a large energy gap between the nonmagnetic ground state and the magnetic excited state in **1**. A diamagnetic dimer showing weak Curie/Weiss-type paramagnetism was also reported by Almeida and coworkers [9]. The positive temperature-independent paramagnetic susceptibilities arise from van Vleck mechanism, which is related to the coupling of the ground and excited states through a magnetic field [43].

In $[M(mnt)_2]^-$ (M = Ni, Pd, and Pt), magnetic property investigations for $[Pd(mnt)_2]^-$ compounds are sparse compared to $[Ni(mnt)_2]^-$ and $[Pt(mnt)_2]^-$. Compounds with eclipsed $[Pd(mnt)_2]_2^{2-}$ dimer pair show diamagnetism or strongly antiferromagnetic coupling behavior [21, 22, 44, 45], probably related to efficient overlap of frontier orbitals of two monomers within a $[Pd(mnt)_2]_2^{2-}$ dimer.

To better understand the magnetic behavior of **1**, the broken-symmetry (BS) DFT approach was employed to evaluate magnetic exchange constants. The BS formalism, originally developed by Noodleman for SCF methods [46], involves a variational treatment

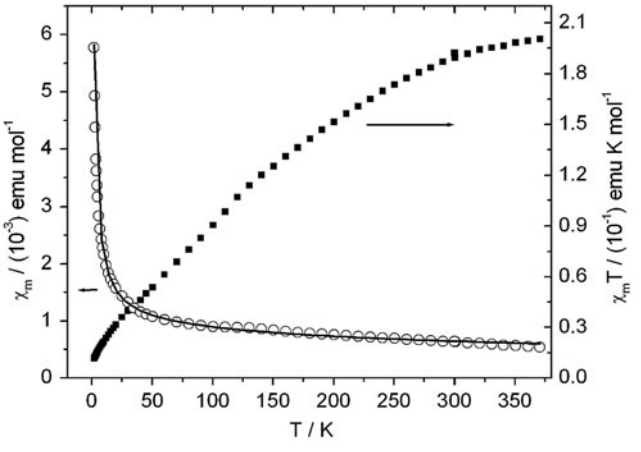

Figure 5. Plots of χ_m *vs.* T and χ_mT *vs.* T for **1** (squares and circles: experimental data; line: theoretical reproduced curve using Curie–Weiss equation).

within the restrictions of a single-spin-unrestricted Slater determinant built upon using different orbitals for different spin. This approach has been applied within the framework of DFT as a practical tool to investigate magnetic interactions on rather large systems (e.g. polynuclear, 1-, 2- and 3-D spin systems) [47–50] with reasonable accuracy and partial consideration of electron correlation effects [51, 52]. For the possible pathways in a studied spin system, calculated energies for the high-spin triplet and BS states of the spin dimers associated with the spin exchange paths (i.e. the structural units consisting of two adjacent magnetic sites) were combined to estimate the exchange constant J involved in the Heisenberg-Dirac-van Vleck Hamiltonian [53–55]:

$$\hat{H} = -2J\vec{S}_1\vec{S}_2 \tag{2}$$

where $\vec{S}_1$ and $\vec{S}_2$ are the respective spin angular momentum operators and J is the magnetic exchange constant between two coupled magnetic centers. A positive sign of J indicates a ferromagnetic (FM) interaction, whereas negative an AFM interaction. Assuming the so-called "weak bonding" regime, Noodleman *et al.* [56–58] evaluated J values within BS framework by

$$J^{(1)} = \frac{E_{\mathrm{BS}} - E_{\mathrm{T}}}{S_{\max}^2} \tag{3}$$

where E_{BS} and E_{T} denote the total energies in the BS singlet state and triplet state, respectively, and $S_{\max}$ corresponds to the total spin of the high-spin state. The following expression might give more reasonable solutions in the strong overlap region [59, 60]:

$$J^{(2)} = \frac{E_{\mathrm{BS}} - E_{\mathrm{T}}}{S_{\max}(S_{\max}+1)} \tag{4}$$

However, Yamaguchi *et al.* claimed that J obtained by the approximate spin projection procedure reproduces the characteristic feature of J in the whole region [51, 61, 62]:

$$J^{(3)} = \frac{E_{\mathrm{BS}} - E_{\mathrm{T}}}{\langle S^2\rangle_{\mathrm{T}} - \langle S^2\rangle_{\mathrm{BS}}} \tag{5}$$

The $\langle S^2\rangle_{\mathrm{T}}$ and $\langle S^2\rangle_{\mathrm{BS}}$ in equation (5) denote the total spin angular momentum of triplet state and BS singlet state, respectively.

In the crystal of **1**, there are three types of magnetic coupling pathways, which involve two neighboring $[\mathrm{TTF}]^+$ cations, two neighboring $[\mathrm{Pd(mnt)_2}]^-$ anions, or the neighboring $[\mathrm{TTF}]^+$ cation and $[\mathrm{Pd(mnt)_2}]^-$ anion. From the structural viewpoint, the magnetic couplings between neighboring magnetic centers are much stronger within a mixed stack than between the inter-stacks since the π-orbital overlap is much greater in the former case than in the latter case; thus, calculations were only performed for the magnetic exchange pathways within a mixed stack. Calculated $\langle S^2\rangle_{\mathrm{T}}$ and $\langle S^2\rangle_{\mathrm{BS}}$ values as well as J values obtained from equation (3) to equation (5) are summarized in table 3, from which it can be found that calculated J values for each spin dimer utilizing equation (3) and equaqtion (5) are close to each other.

The calculations reveal the existence of strong antiferromagnetic coupling within the $[\mathrm{Pd(mnt)_2}]_2^{2-}$ dimer and $[\mathrm{TTF}]_2^{2+}$ dimer, with weak ferromagnetic coupling between

Table 3. Calculated $\langle S^2\rangle_T$ and $\langle S^2\rangle_{BS}$ as well as J values for each spin dimer in the crystal of **1**.

Spin dimer	$J^{(1)}/k_B$ (K)	$J^{(2)}/k_B$ (K)	$J^{(3)}/k_B$ (K)	$\langle S^2\rangle_T$	$\langle S^2\rangle_{BS}$
$[Pd(mnt)_2]_2^{2-}$	−7835	−3918	3912	2.0029	0.0000
$[TTF]_2^{2+}$	−8178	−4089	4087	2.0012	0.0000
$[TTF]^+[Pd(mnt)_2]^-$	194	97	97	2.0022	0.0000

Notes: $J^{(1)}/k_B$, $J^{(1)}/k_B$ and $J^{(1)}/k_B$ are calculated using equations (3)–(5), respectively.

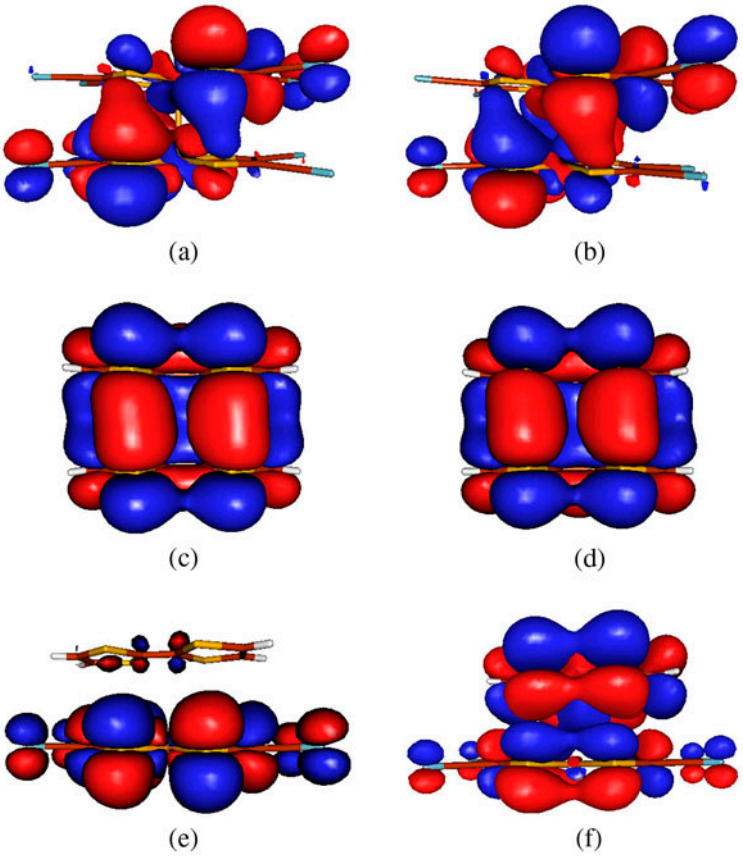

Figure 6. Calculated α (left) and β (right) SOMO for the BS singlet states of (a, b) the $[Pd(mnt)_2]_2^{2-}$ dimer, (c, d) the $[TTF]_2^{2+}$ dimer and for the triplet state of (e, f) the $[TTF]^+[Pd(mnt)_2]^-$, respectively.

neighboring anion and cation. Figure 6 shows the frontier molecule orbitals of the BS states of $[Pd(mnt)_2]_2^{2-}$ and $[TTF]_2^{2+}$ spin dimers, and the triplet state of $[TTF]^+[Pd(mnt)_2]^-$, which further identify the existence of strong overlap in $[Pd(mnt)_2]_2^{2-}$ and $[TTF]_2^{2+}$, and weak overlap in $[TTF]^+[Pd(mnt)_2]^-$. The greater frontier orbital overlap in $[Pd(mnt)_2]_2^{2-}$ and $[TTF]_2^{2+}$ spin dimers leads to stronger antiferromagnetic coupling within the dimers, which gives a large value of energy gap between the nonmagnetic ground state and the magnetic excited state. The spin polarization results in weak ferromagnetic coupling between $[TTF]^+$ and $[Pd(mnt)_2]^-$.

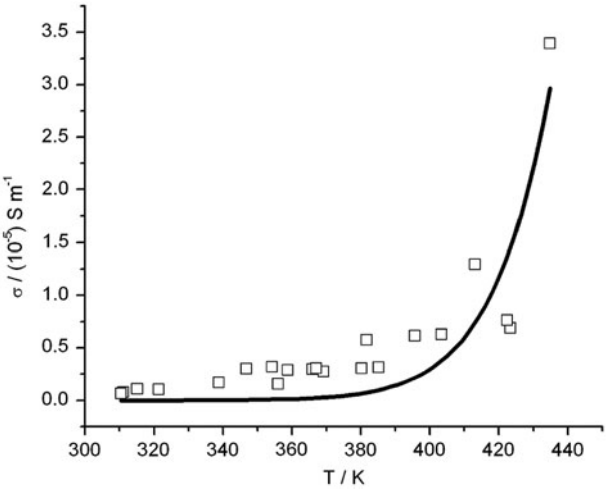

Figure 7. Plot of lnσ-1000/T for **1** from 310 to 435 K (38–162 °C) (squares: experimental data and line: theoretically reproduced plot using Arrhenius equation).

3.3. *Electrical conductivity*

It is difficult to prepare sufficient-size crystal for the measurement of single-crystal electronic transport owing to the insolubility of **1**. Thus, the four-probe electrical conductivity measurement was performed for the compressed powder pellet. The plot of temperature-dependent electrical conductivity (σ) is displayed in figure 7 for **1**, indicating $\sigma = 6.5 \times 10^{-7}\,\mathrm{S\,cm^{-1}}$ at 310 K (38 °C) and semiconductor character from 310 to 435 K (38–160 °C). The fit for the temperature-dependent electrical conductivity, using the Arrhenius equation, gave activation energy of 1.1(3) eV.

4. Conclusion

We prepared a new ion-pair compound consisting of $[TTF]^+$ and $[Pd(mnt)_2]^-$. The $[TTF]^+$ (C) and $[Pd(mnt)_2]^-$ (A) form mixed stacks in …AACCAACC… fashion in the crystal. This ion-pair compound shows weak Curie/Weiss-type magnetic behavior, which results from strong antiferromagnetic coupling in both $[Pd(mnt)_2]_2^{2-}$ and $[TTF]_2^{2+}$ dimers, via the frontier orbitals overlap mechanism, within a mixed stack. The ion-pair compound shows semiconductor character with activation energy of 1.1(3) eV.

Supplementary material

Crystallographic data in CIF format for **1** is available free of charge via the Internet.

Acknowledgments

Authors thank the Science and Technology Department of Jiangsu Province and National Natural Science Foundation of China for financial support (Grant Nos. BK2010551 and 21271103).

References

[1] A.T. Coomber, D. Beljonne, R.H. Friend, J.L. Bredas, A. Charlton, N. Robertson, A.E. Underhill, M. Kurmoo, P. Day. *Nature*, **380**, 144 (1996).
[2] I.D. Parker, R.H. Friend, P.I. Clemenson, A.E. Underhill. *Nature*, **324**, 547 (1986).
[3] J. Nishijo, E. Ogura, J. Yamaura, A. Miyazaki, T. Enoki, T. Takano, Y. Kuwatani, M. Iyoda. *Solid State Commun.*, **116**, 661 (2000).
[4] A.E. Pullen, C. Faulmann, K.I. Pokhodnya, P. Cassoux, M. Tokumoto. *Inorg. Chem.*, **37**, 6714 (1998).
[5] D. Arcoõn, A. Lappas, S. Margadonna, K. Prassides. *Phys. Rev. B*, **60**, 4191 (1999).
[6] E. Ribera, C. Rovira, J. Veciana, J. Tarrés, E. Canadell, R. Rousseau, E. Molins, M. Mas, J.-P. Schoeffel, J.-P. Pouget, J. Morgado, R.T. Henriques, M. Almeida. *Chem. Eur. J.*, **5**, 2025 (1999).
[7] J.C. Dias, X. Ribas, J. Morgado, J. Seica, E.B. Lopes, I.C. Santos, R.T. Henriques, M. Almeida, K. Wurst, P. Foury-Leylekian, E. Canadell, J. Vidal-Gancedo, J. Veciana, C. Rovira. *J. Mater. Chem.*, **15**, 3187 (2005).
[8] X. Ribas, A. Sironi, N. Masciocchi, E.B. Lopes, M. Almeida, J. Veciana, C. Rovira. *Inorg. Chem.*, **44**, 2358 (2005).
[9] R.A.L. Silva, M.L. Afonso, I.C. Santos, D. Belo, R.R. Freitas, E.B. Lopes, J.T. Coutinho, L.C.J. Pereira, R.T. Henriques, M. Almeida, C. Rovira. *Phys. Status Solidi C*, **9**, 1134 (2012).
[10] L.C. Isett, D.M. Rosso, G.L. Bottger. *Phys. Rev. B*, **22**, 4739 (1980).
[11] P.I. Clemenson, A.E. Underhill, M.B. Hursthouse, R.L. Short. *J. Chem. Soc., Dalton Trans.*, 1689 (1988).
[12] A.E. Underhill, M.M. Ahmad. *J. Chem. Soc., Chem. Commun.*, 67 (1981).
[13] M.M. Ahmad, D.J. Turner, A.E. Underhill, C.S. Jacobsen, K. Mortensen, K. Carneiro. *Phys. Rev. B*, **29**, 4796 (1984).
[14] X.M. Ren, Q.J. Meng, Y. Song, C.J. Hu, C.S. Lu, X.Y. Chen. *Inorg. Chem.*, **41**, 5686 (2002).
[15] J.L. Xie, X.M. Ren, Y. Song, W.W. Zhang, W.L. Liu, C. He, Q.J. Meng. *Chem. Commun.*, **2**, 2346 (2002).
[16] J.L. Xie, X.M. Ren, C. He, Z.M. Gao, Y. Song, Q.J. Meng, R.K. Kremer. *Chem. Phys. Lett.*, **369**, 41 (2003).
[17] X.M. Ren, T. Akutagawa, S. Nishihara, T. Nakamura, W. Fujita, K. Awaga. *J. Phys. Chem. B*, **109**, 16610 (2005).
[18] D.B. Dang, C.L. Ni, Y. Bai, Z.F. Tian, Z.P. Ni, L.L. Wen, Q.J. Meng, S. Gao. *Chem. Lett.*, **34**, 680 (2005).
[19] Z.F. Tian, H.B. Duan, X.M. Ren, C.S. Lu, Y.Z. Li, Y. Song, H.Z. Zhu, Q.J. Meng. *J. Phys. Chem. B*, **113**, 8278 (2009).
[20] X.M. Ren, H. Okudera, R.K. Kremer, Y. Song, C. He, Q.J. Meng, P.H. Wu. *Inorg. Chem.*, **43**, 2569 (2004).
[21] X.M. Ren, T. Akutagawa, S. Nishihara, T. Nakamura. *Synth. Met.*, **150**, 57 (2005).
[22] X.M. Ren, H. Okudera, J.L. Xie, Q.J. Meng. *J. Mol. Struct.*, **733**, 119 (2005).
[23] J.M. Williams, J.R. Ferraro, R.J. Thorn, K.D. Carlson, U. Geiser, H.H. Wang, M.A. Kini, M.-H. Whangbo. *Organic Superconductors* (Including Fullerenes), Prentice-Hall, Englewood Cliffs, NJ (1992).
[24] J.W. Bray, H.R. Hart, Jr., L.V. Interrante, I.S. Jacobs, J.S. Kasper, G.D. Watkins, S.H. Wee, J.C. Bonner. *Phys. Rev. Lett.*, **35**, 744 (1975).
[25] I.S. Jacobs, J.W. Bray, H.R. Hart, Jr., L.V. Interrante, J.S. Kasper, G.D. Watkins, D.E. Prober, J.C. Bonner. *Phys. Rev. B*, **14**, 3036 (1976).
[26] S. Wang, W. He, W. Huang. *J. Chem. Crystallogr.*, **41**, 430 (2011).
[27] F. Wull. *J. Am. Chem. Soc.*, **97**, 1962 (1975).
[28] A. Davison, H.R. Holm. *Inorg. Synth.*, **10**, 8 (1967).
[29] M.J. Frisch, G.W. Trucks, H.B. Schlegel, G.E. Scuseria, M.A. Robb, J.R. Cheeseman, V.G. Zakrzewski, J.A. Montgomery, Jr., R.E. Stratmann, J.C. Burant, S. Dapprich, J.M. Millam, A.D. Daniels, K.N. Kudin, M.C. Strain, O. Farkas, J. Tomasi, V. Barone, M. Cossi, R. Cammi, B. Mennucci, C. Pomelli, C. Adamo, S. Clifford, J. Ochterski, G.A. Petersson, P.Y. Ayala, Q. Cui, K. Morokuma, P. Salvador, J.J. Dannenberg, D.K. Malick, A.D. Rabuck, K. Raghavachari, J.B. Foresman, J. Cioslowski, J.V. Ortiz, A.G. Baboul, B.B. Stefanov, G. Liu, A. Liashenko, P. Piskorz, I. Komaromi, R. Gomperts, R.L. Martin, D.J. Fox, T. Keith, M.A. Al-Laham, C.Y. Peng, A. Nanayakkara, M. Challacombe, P.M.W. Gill, B. Johnson, W. Chen, M.W. Wong, J.L. Andres, C. Gonzalez, M. Head-Gordon, E.S. Replogle, J.A. Pople. *Gaussian 98*, *Revision A.11*, Gaussian, Pittsburgh, PA. (2001).
[30] A.D. Becke. *Phys. Rev. A*, **38**, 3098 (1988).
[31] K. Burke, J.P. Perdew, Y. Wang. In *Electronic Density Functional Theory: Recent Progress and New Directions*, J.F. Dobson, G. Vignale, M.P. Das (Eds.), p. 81, Plenum Publishing, New York (1998).
[32] J.P. Perdew. In *Electronic Structure of Solids'91*, P. Ziesche, H. Eschrig (Eds.), p. 11, Akademie Verlag, Berlin (1991).
[33] J.P. Perdew, J.A. Chevary, S.H. Vosko, K.A. Jackson, M.R. Pederson, D.J. Singh, C. Fiolhais. *Phys. Rev. B*, **46**, 6671 (1992).
[34] J.P. Perdew, J.A. Chevary, S.H. Vosko, K.A. Jackson, M.R. Pederson, D.J. Singh, C. Fiolhais. *Phys. Rev. B*, **48**, E4978 (1993).
[35] J.P. Perdew, K. Burke, Y. Wang. *Phys. Rev. B*, **54**, 16533 (1996).
[36] Software packages. *SMART and SAINT*, Siemens Analytical X-ray Instrument, Madison, WI (1996).

[37] G.M. Sheldrick. *SHELXL-97, Program for the Refinement of Crystal Structure*, University of Göttingen, Germany (1997).
[38] W.B. Pei, J.L. Liu, J.S. Wu, X.M. Ren, D.W. Gu, L.J. Shen, Q.J. Meng. *J. Mol. Struct.*, **918**, 160 (2009).
[39] H. Bois, N.G. Connelly, J.G. Crossley, J.-C. Guillorit, G.R. Lewis, A.G. Orpen, P. Thornton. *J. Chem. Soc., Dalton Trans.*, 2833 (1998).
[40] J.S. Wu, W.B. Pei, L.J. Shen. *Synth React Inorg. Met.-Org. Nano-Met. Chem.*, **41**, 852 (2011).
[41] M.B. Hursthouse, R.L. Short, P.I. Clemenson, A.E. Underhill. *J. Chem. Soc., Dalton Trans.*, 67 (1989).
[42] M.B. Hursthouse, R.L. Short, P.I. Clemenson, A.E. Underhill. *J. Chem. Soc., Dalton Trans.*, **12**, 1101 (1989).
[43] J.H. van Vleck. *The Theory of Electric and Magnetic Susceptibilities*, Oxford, London (1932).
[44] M. Uruichi, K. Yakushi, Y. Yamashita, J. Qin. *J. Mater. Chem.*, **8**, 141 (1998).
[45] A. Davison, N. Edelstein, R.H. Holm, A.H. Maki. *Inorg. Chem.*, **2**, 1227 (1963).
[46] L. Noodleman, J.G. Norman, Jr. *J. Chem. Phys.*, **70**, 4903 (1979).
[47] R. Singh, A. Banerjee, E. Colacio, K.K. Rajak. *Inorg. Chem.*, **48**, 4753 (2009).
[48] J.L. Manson, M.M. Conner, J.A. Schlueter, A.C. McConnell, H.I. Southerland, I. Malfant, T. Lancaster, S.J. Blundell, M.L. Brooks, F.L. Pratt, J. Singleton, R.D. McDonald, C. Lee, M.-H. Whangbo. *Chem. Mater.*, **20**, 7408 (2008).
[49] J.L. Manson, J.A. Schlueter, K.A. Funk, H.I. Southerland, B. Twamley, T. Lancaster, S.J. Blundell, P.J. Baker, F.L. Pratt, J. Singleton, R.D. McDonald, P.A. Goddard, P. Sengupta, C.D. Batista, L. Ding, C. Lee, M.-H. Whangbo, I. Franke, S. Cox, C. Baines, D. Trial. *J. Am. Chem. Soc.*, **131**, 6733 (2009).
[50] M. Mitsumi, Y. Yoshida, A. Kohyama, Y. Kitagawa, Y. Ozawa, M. Kobayashi, K. Toriumi, M. Tadokoro, N. Ikeda, M. Okumura, M. Kurmoo. *Inorg. Chem.*, **48**, 6680 (2009).
[51] H. Nagao, M. Nishino, Y. Shigeta, T. Soda, Y. Kitagawa, T. Onishi, Y. Yoshioka, K. Yamaguchi. *Coord. Chem. Rev.*, **198**, 265 (2000).
[52] I. Ciofini, C.A. Daul. *Coord. Chem. Rev.*, **187**, 238 (2003).
[53] W. Heisenberg. *Z. Phys.*, **49**, 619 (1928).
[54] P.A.M. Dirac. *The Principles of Quantum Mechanics*, Clarendon Press, Oxford, UK (1947).
[55] J.H. Van Vleck. *The Theory of Electric and Magnetic Susceptibilities*, Oxford University Press, Oxford, UK (1932).
[56] A.P. Ginsberg. *J. Am. Chem. Soc.*, **102**, 111 (1980).
[57] L. Noodleman. *J. Chem. Phys.*, **74**, 5737 (1981).
[58] L. Noodleman, E.R. Davidson. *Chem. Phys.*, **109**, 131 (1986).
[59] A. Bencini, F. Totti, C.A. Daul, K. Doclo, P. Fantucci, V. Barone. *Inorg. Chem.*, **36**, 5022 (1997).
[60] E. Ruiz, J. Cano, S. Alvarez, P. Alemany. *J. Comput. Chem.*, **20**, 1391 (1999).
[61] T. Soda, Y. Kitagawa, T. Onishi, Y. Takano, Y. Shigeta, H. Nagao, Y. Yoshioka, K. Yamaguchi. *Chem. Phys. Lett.*, **319**, 223 (2000).
[62] Y. Takano, Y. Kitagawa, T. Onishi, Y. Yoshioka, K. Yamaguchi, N. Koga, H. Iwamura. *J. Am. Chem. Soc.*, **124**, 450 (2002).